I&EC research
Industrial & Engineering Chemistry Research

Article

pubs.acs.org/IECR

Thermal Diffusivity and Viscosity of Suspensions of Disk-Shaped Nanoparticles

Susheel S. Bhandari and K. Muralidhar

Department of Mechanical Engineering, Indian Institute of Technology Kanpur, Kanpur 208016 India

Yogesh M. Joshi*

Department of Chemical Engineering, Indian Institute of Technology Kanpur, Kanpur 208016 India

ABSTRACT: In this work we conduct a transient heat conduction experiment with an aqueous suspension of nanoparticle disks of Laponite JS, a sol forming grade, using laser light interferometry. The image sequence in time is used to measure the thermal diffusivity and thermal conductivity of the suspension. Imaging of the temperature distribution is facilitated by the dependence of the refractive index of the suspension on temperature itself. We observe that with the addition of 4 vol % nanodisks in water, the thermal conductivity of the suspension increases by around 30%. A theoretical model for the thermal conductivity of the suspension of anisotropic particles by Fricke as well as by Hamilton and Crosser explains the trend of data well. In turn, it estimates the thermal conductivity of the Laponite nanoparticle itself, which is otherwise difficult to measure in a direct manner. We also measure the viscosity of the nanoparticle suspension using a concentric cylinder rheometer. Measurements are seen to follow quite well the theoretical relation for the viscosity of suspensions of oblate particles that includes up to two-particle interaction. This result rules out the presence of clusters of particles in the suspension. The effective viscosity and thermal diffusivity data show that the shape of the particle has a role in determining the enhancement of thermophysical properties of the suspension.

I. INTRODUCTION

Diffusion of momentum and heat in liquids containing suspended colloidal particles is of significant academic importance and has many technological applications. It is known that suspension of solid particles in liquid media enhances its viscosity (i.e., momentum diffusivity) and influences thermal diffusivity.[1] The changes in viscosity and thermal diffusivity of the suspension mainly depend on the shape and size of the suspended particles.[2−4] In addition, the nature of the surface such as charge, its distribution, and the presence of surfactant plays an important role.[5,6] It has been noted that suspensions of anisotropic particles tend to show greater viscosity, namely, momentum diffusivity, as well as enhanced thermal diffusivity, compared to isotropic, spherelike, particles for a given volume fraction.[2,3,7−10] However, much less work has been carried out in the literature to study the behavior of suspensions of anisotropic particles in comparison to the isotropic. Specifically, among suspensions of anisotropic particles, very few studies investigate suspensions of disklike (oblate) particles compared to those of rodlike (prolate) particles. Owing to greater demand for effective thermal transport from different kinds of devices whose length scales range over 6 orders of magnitude (micrometers to meters), this is a continuing area of research.

The subject of heat transport through dilute suspensions of solid particles has received a renewed boost owing to reports of enhancement in thermal conductivity of suspensions carrying nanoparticles.[8−11] This increase is well beyond what is predicted by theoretical formulations that have been validated and known to work well for stable suspensions of larger particles. Such an anomalous increase in thermal conductivity has been attributed by various authors to factors such as enhanced Brownian diffusivity,[12] phonon transport,[11] layering of liquid molecules over the particle surface,[13] and fractal cluster formation.[6,14] Recent literature, however, indicates a consensus on the possibility of cluster formation of nanoparticles as the factor responsible for the anomalous enhancement in thermal conductivity.[9] A major limitation in many studies that analyze enhancement of thermal conductivity in nanofluids by using theoretical models is the unavailability of thermal conductivity of the nanoparticles. In such cases assumption of thermal conductivities over a certain range facilitates comparison of the trend. Interestingly, careful and independent investigations on this subject do not subscribe to the claim of anomalous enhancement of thermal conductivity beyond the theoretical.[15,16] Poulikakos and co-workers[15] carefully studied the effect of particle size, concentration, method of stabilization, and clustering on thermal transport in gold nanofluid. A maximum enhancement of 1.4% was reported for 0.11 vol % suspension of 40 nm diameter particles in water, suggesting no apparent anomaly.

In general, if the thermal conductivity of the suspended particles is significantly greater than that of the suspending liquid, an increase in the aspect ratio is expected to cause substantial enhancement in the thermal conductivity of the

Received: August 1, 2013
Revised: October 1, 2013
Accepted: October 4, 2013
Published: October 4, 2013

dx.doi.org/10.1021/ie402508x | *Ind. Eng. Chem. Res.* 2013, 52, 15114−15123

suspension. This is due to the fact that, for the same volume fraction, anisotropy allows thermal transport over greater length scales through elongated shape and greater surface area of the suspended particles. Here, the aspect ratio is defined in such a way that it is less than unity for oblate particles and greater than unity for the prolate. Based on Hamilton and Crosser theory,[3] Keblinski and co-workers[17] suggested that, for equal volume fractions, a 10-fold enhancement in thermal conductivity is obtained when the aspect ratio of the anisotropic particle is around 100 (or 1/100). A good amount of work has been carried out in the literature to investigate thermal properties of carbon nanotube suspensions in a variety of solvents.[8−11] Owing to different aspect ratios, solvents, and type of nanotubes (single or multiwall), there is considerable spread in the data. The reported values range from 10% to over 150% enhancement in the thermal conductivity for 1 vol % concentration.[13,18−23] On the other hand, experiments with an aqueous suspension of titanate nanotubes having an aspect ratio of 10 are reported to show a very moderate enhancement of around 3% for 2.5 wt % suspension.[24] Recently, Cherkasova and Shan[25] studied the thermal conductivity behavior of suspension of whiskers having various aspect ratios (up to 10) and observed that, for a constant total volume fraction, thermal conductivity increases with increase in the aspect ratio. The experimental data showed good agreement with the effective medium theory of Nan and co-workers[26] which accounts for interfacial resistance in the conventional theories.

Compared to suspensions of rodlike particles, less work has been reported for suspensions of disklike particles. Singh and co-workers[27] studied the heat transfer behavior of an aqueous suspension of silicon carbide having an oblate shape and an aspect ratio of around 1/4. They typically observed 30% enhancement for 7 vol % concentration. The authors analyzed the data using Hamilton and Crosser theory[3] and found a correlation between them. Khandekar and co-workers[28] employed various spherical nanoparticles as well as Laponite JS (oblate shape, aspect ratio 1/25) based nanofluids in a closed two phase thermosyphon and observed their heat transport behavior to be inferior to that of pure water in all cases. However, in a thermosyphon, in addition to thermal conductivity, fluid viscosity, wettability of the liquid on the surface of the apparatus, and roughness of the surface compared to particle dimensions also play an important role.[28] Recently, Bhandari and co-workers[29] reported transient the heat transport behavior of a suspension of gel forming grade of nanoclay called Laponite RD, which has a soft solidlike consistency. Interestingly, for about 1 vol % concentration of clay, over 30% enhancement in thermal conductivity was observed. Unlike the previous examples, this system is in solid state with a finite elastic modulus (and infinite viscosity).[29] Recently, many groups have studied heat transport in nanofluids composed of graphene. It has negligible thickness compared to its lateral dimensions and an extreme aspect ratio. Most studies employ water as the suspending medium. In order to render graphene hydrophilic, a functionalization step is carried out. For functionalized graphene−water nanofluids, thermal conductivity enhancement of 15−25% is observed for around 0.05 vol %.[30−32] Other studies employ water-soluble solvents such as ethylene glycol[33] and alcohol[34] and report similar enhancements as for water. Although most studies on graphene nanofluid report thermal conductivity enhancement with increased temperature,[30−32,35] one study reports that it remains constant.[34] Dhar et al.[36] and Martin-Gallego et al.[37] have analyzed thermal conductivity enhancement in graphene nanofluid and emphasized the importance of phonon transport. Two studies have compared the effect of particle shape, namely, prolate vis á vis oblate on the thermal conductivity enhancement at a given concentration using carbon nanotubes and graphene nanofluids. Interestingly, Martin-Gallego et al.[37] observe enhancement in both systems to be comparable while Wang and co-workers[35] report that graphene nanofluid performs better than nanotube suspension.

In the present work, we study transient heat transport behavior of an aqueous suspension of sol forming nanoclay Laponite JS, which is an anisotropic, disk-shaped nanoparticle, using laser light interferometry.

II. VISCOSITY AND THERMAL CONDUCTIVITY OF SUSPENSION OF OBLATE SPHEROIDS

In the limit of very low volume fractions ($\phi < 0.03$), an expression of the viscosity of a suspension having spherical particles is due to Einstein and is given by[38]

$$\eta = \eta_s(1 + 2.5\phi)$$

where η_s is the viscosity of the Newtonian solvent in which the particles having volume fraction ϕ are suspended. This expression was obtained by estimating dissipation associated with flow around the sphere and assumes that the flow field around one sphere is not influenced by the presence of other spheres in the vicinity (therefore, the dilute limit). This expression was modified by incorporating hydrodynamic interactions associated with two-body interactions by Batchelor and Green.[39] The two-body interaction leads to a contribution to η proportional to ϕ^2.

For a suspension containing monodispersed particles, the general expression for low shear viscosity irrespective of the aspect ratio of the particles can be written as[40,41]

$$\eta_r = \frac{\eta}{\eta_s} = 1 + C_1\phi + C_2\phi^2 + O(\phi^3) \quad (1)$$

where C_1 and C_2 respectively represent one- and two-body interactions and the volume fraction ϕ. In this expression, $C_1 = [\eta]_0$ and $C_2 = k_H[\eta]_0^2$, where $[\eta]_0$ is an intrinsic viscosity in the limit of low shear rates. Parameter k_H is the Huggins coefficient, which relates viscosity originating from two-body interactions to that of viscosity associated with the infinite dilution limit where two-body interactions are negligible. For particles having hard core interactions, the theoretical value of Huggins coefficient has been estimated to be $k_H \approx 1$ for spheres.[40] A theoretical value for disklike particles is not available in the literature. Equation 1 with up to two-body interaction (ϕ^2 term) term holds good for $\phi \leq 0.1$.

In this work we study the viscosity behavior of oblate spheroidal particles. We assume d and a to be the length scales associated with the short and long axes of the spheroid, respectively. For a disk, d and a can be considered as the thickness and diameter, respectively. Intrinsic viscosity $[\eta]_0$, a dimensionless quantity, is a function of the aspect ratio r_p ($=d/a < 1$) and is given by the expression[41,42]

$$[\eta]_0 = \frac{5}{2} + \frac{32}{15\pi r_p}(1 - r_p) - 0.628\left(\frac{1 - r_p}{1 - 0.075r_p}\right) \quad (2)$$

It can be seen that the intrinsic viscosity expressed by eq 2 is sensitive to the aspect ratio of the particle. It is inherently

dx.doi.org/10.1021/ie402508x | Ind. Eng. Chem. Res. 2013, 52, 15114−15123

assumed in eqs 1 and 2 that particle orientation is isotropic, and therefore these equations are applicable only in the limit of small rotational Peclet number ($Pe \ll 1$) defined as[38]

$$Pe = \frac{4\eta_s d^3 \dot{\gamma}}{3kT} \tag{3}$$

In eq 3, $\dot{\gamma}$ is the shear rate, k is the Boltzmann constant, η_s is the solvent viscosity, and T is temperature.

The expression for the electrical conductivity of a suspension containing oblate nonpolarizable spheroidal particles is due to Fricke.[2] In this analysis, a single particle was placed in a unit cell, subjected to a unit potential difference, and analyzed in terms of Poisson's equation for a two-phase system. The influence of all other particles in the suspension on the near field of the single particle was taken to be equal to the mean value for the entire suspension. The prediction of electrical conductivity was seen to match very well with that of dog's blood for concentrations of red corpuscles up to 90% in serum, with the particles being treated as oblate spheroids. Treating thermal conductivity as analogous to electrical conductivity, the effective thermal conductivity of a suspension containing oblate spheroidal particles is given by[2,25]

$$k_e = k_s\left[\frac{\zeta + (n-1) + (n-1)(\zeta-1)\phi}{\zeta + (n-1) - (\zeta-1)\phi}\right] \tag{4}$$

where k_s is the thermal conductivity of the solvent, $\zeta = k_p/k_s$ is the particle-to-solvent conductivity ratio, and k_p is the thermal conductivity of the particles. Parameter n is a shape factor given by

$$n = \frac{\beta(\zeta-1)}{(\zeta-1) - \beta} \tag{5}$$

Here β is

$$\beta = \frac{1}{3}\left[\frac{4(\zeta-1)}{2 + M(\zeta-1)} + \frac{\zeta-1}{1 + (1-M)(\zeta-1)}\right] \tag{6}$$

and

$$M = \frac{2\varphi - \sin 2\varphi}{2\sin^3\varphi}\cos\varphi \tag{7}$$

where $\varphi = \cos^{-1}(r_p)$.

Rather than extending the expression derived for electric conductivity to thermal conductivity as carried out by Fricke,[2] Hamilton and Crosser[3] obtained effective the thermal conductivity of a two-component heterogeneous system by expressing it in terms of ratios of the average temperature gradient in both phases. They obtained the average gradient ratio by using expressions developed by Maxwell[7] and Fricke,[2] which led to the identical expression for k_e as given by eq 4 but a different shape factor:[3]

$$n = 3/\Psi \tag{8}$$

where Ψ is the sphericity expressed as the ratio of the surface area of a sphere having the same volume as the particle to that of the surface area of the particle. For a disk having diameter a and thickness d (aspect ratio $r_p = d/a$), sphericity is given by the expression

$$\Psi = \frac{2(3r_p/4)^{2/3}}{1 + r_p} \tag{9}$$

The major difference between the analyses of Fricke and Hamilton and Crosser is the way effect of the shape is incorporated. The latter considers the shape factor to be an empirical constant and expresses it as $n = 3/\Psi$. On the other hand, in the Fricke expression the shape factor is a function of the thermal conductivities of the particle and the base fluid in addition to the aspect ratio. The expression by Hamilton and Crosser shows the thermal conductivity of a suspension to be slightly higher than that of Fricke for a given volume fraction of suspended particles. Both expressions yield the Maxwell relation in the limit of spherical shape of the particle (aspect ratio of unity).

Similar to the expression for viscosity, a necessary condition for the application of the Fricke model as well as the Hamilton and Crosser model is an isotropic distribution of orientations of the disk-shaped particles. This requirement is ensured at the low Peclet number limit ($Pe \ll 1$). In addition, sufficient time is needed to be given to the suspension in an experiment to stabilize so that Brownian motions randomize the orientation of clay disks and erase the shear history.

While the Fricke model is for electrical conductivity, it has been used to estimate thermal conductivity from the following thermodynamic perspective. Natural phenomena follow a cause−effect relationship that is expressible as in terms of forces and fluxes. It is a linear relation for electrical, thermal, hydraulic, and other situations. Thus, one can have expressions for electrical, thermal, and hydraulic resistances and conductivities. Though the conductivities do not match in dimensional form, we can expect nondimensional conductivities of thermal and electrical systems scaled by a reference to match in quantitative terms.

III. DETERMINATION OF THERMAL DIFFUSIVITY FROM AN UNSTEADY EXPERIMENT

Consider a horizontal layer of the aqueous suspension in one dimension of thickness H maintained initially at constant temperature T_C. At time $t > 0$, the temperature of the top surface is suddenly raised to T_H ($>T_C$). Consequently, heat diffuses from the top plate toward the bottom plate. The configuration is gravitationally stable in density. Hence, convection currents are absent and heat transfer is determined by pure diffusion. Combining Fourier's law of heat conduction with the first law of thermodynamics, the governing equation for temperature is given by[1]

$$\frac{\partial\theta}{\partial\tau} = \frac{\partial^2\theta}{\partial\psi^2} \tag{10}$$

Here $\theta = (T - T_C)/(T_H - T_C)$ is dimensionless temperature, $\tau = \alpha t/H^2$ is dimensionless time, and $\psi = y/H$ is a dimensionless coordinate measured from the lower surface. In addition, t is time and α is the thermal diffusivity of the suspension. The initial and boundary conditions associated with eq 10 are[29]

$$\begin{aligned} &\theta = 0 \quad \tau \le 0 \\ &\theta = 1 \quad \tau > 0, \ \psi = 1 \\ &\theta = 0 \quad \tau > 0, \ \psi = 0 \end{aligned} \tag{11}$$

Equation 10 can be analytically solved for a constant thermal diffusivity medium subject to conditions described by eq 11 to yield[29]

dx.doi.org/10.1021/ie402508x | Ind. Eng. Chem. Res. 2013, 52, 15114−15123

$$\theta = \psi - 2\sum_{n}[(-1)^{n+1}/n\pi]\sin(n\pi\psi)\exp(-n^2\pi^2\tau),$$
$$\text{for } n = 1, 2, 3, \ldots \quad (12)$$

Over the range of temperatures discussed in section IV, thermal diffusivity changes by less than 0.5% and the constant diffusivity approximation is valid. According to eq 12, the only material property that fixes the evolution of the temperature field is thermal diffusivity α.

We describe in section IV the experimental procedure to obtain temperature within the suspension as a function of position (y) and time. Using an inverse technique, we fit eq 12 to the experimentally obtained temperature data to estimate thermal diffusivity. The technique relies on the method of least squares where the variance of the measured temperature relative to the analytical is minimized with respect to diffusivity as a parameter. In the limit of steady state ($\tau \to \infty$), eq 12 becomes independent of thermal diffusivity. Hence, with increase in time, the fit of eq 12 to the experimental data becomes progressively less sensitive to the choice of α. In addition, with the approach of steady state, the temperature field in the aqueous suspension is affected by the thermal properties of the confining surfaces. At the other extreme of small values of τ, temperature gradients near the heated boundary are large and optical measurements are contaminated by refraction errors. Hence, with small time data, the uncertainty associated with the estimated thermal diffusivity from eq 12 is expected to be large. It can be concluded that the regression of experimental data against the analytical solution is most appropriate only at intermediate times. The conventional least-squares procedure is thus modified to an equivalent weighted least-squares procedure to highlight the data within a certain sensitivity interval, as discussed below.

Let a_j ($j = 1, 2, \ldots, m$) parameters be determined from measurement data Y_i ($i = 1, 2, \ldots, n > m$) using a mathematical model $T_i(a_j)$ by a least-squares procedure. The process of minimizing the error functional

$$E(a_j) = \sum_{i-1}^{n}(Y_i - T_i)^2 \quad (13)$$

leads to the system of algebraic equations:[43]

$$\{a_j\} = [J^{\mathrm{T}}J]^{-1}J^{\mathrm{T}}\{Y_i\} \quad (14)$$

Here, J is a Jacobian matrix defined as

$$J_{ij} = \frac{\partial T_i}{\partial a_j} \quad (15)$$

Equation 14 shows that uncertainty in the estimated parameters a_j depends on the condition number of the matrix $J^{\mathrm{T}}J$ since its inverse multiplies the measured data Y_i. Specifically, the condition number should be large for the uncertainty to be small. This requirement leads to the result that the diagonal entries of the matrix $J^{\mathrm{T}}J$ should be large. In this context, the Jacobian is referred to as sensitivity in the literature.[44]

During estimation of a single parameter, namely thermal diffusivity from spatiotemporal data of temperature, sensitivity estimates can be alternatively derived as follows. In analogy to eq 15, the sensitivity parameter for the suspension as a whole is obtained by integrating over the layer thickness and is given by[44]

$$S_t(t, \alpha) = \int_0^H \frac{\partial T}{\partial \alpha}\,\mathrm{d}y \quad (16)$$

By differentiating eq 12, the dimensionless form of the sensitivity parameter $\bar{S}_t$ is given by the expression

$$\bar{S}_t = \frac{\alpha_R S_t}{H(T_H - T_C)} = -2\tau\sum_{n=1}^{\infty}[(-1)^{2n+1} + (-1)^{n+2}]\exp(-\bar{\alpha}n^2\pi^2\tau_R) \quad (17)$$

where α_R is thermal diffusivity of a reference material (water in the present study), $\bar{\alpha} = \alpha/\alpha_R$, and $\tau_R = \alpha_R t/H^2$.

Analogous to time, a fit to the experimental data closer to either of the boundaries in not sensitive to the choice of α. The loss of sensitivity arises from the fact that the walls are at constant temperature, independent of the material diffusivity. Following eq 16, sensitivity associated with the experimental data as a function of the spatial coordinate can be estimated by integrating with respect to time and is given by

$$S_y(y, \alpha) = \int_0^{\infty}\frac{\partial T}{\partial \alpha}\,\mathrm{d}t \quad (18)$$

However, in eq 18 rather than integrating $\partial T/\partial\alpha$ over the entire duration of the experiment, we integrate the same over only that duration where sensitivity estimated from eqs 16 and 17 is very high (typically above 90% of the maximum in sensitivity). If the interval between t_1 and t_2 represents that window of high sensitivity, eq 18 can be modified to

$$S_y(y, \alpha) = \int_{t_1}^{t_2}\frac{\partial T}{\partial \alpha}\,\mathrm{d}t \quad (19)$$

In a manner similar to eq 17, the dimensionless sensitivity parameter $\bar{S}_y$ for spatial sensitivity of data is given by

$$\bar{S}_y = \frac{S_y\alpha_R}{(T_H - T_C)(t_2 - t_1)} = \frac{1}{\bar{\alpha}(\tau_{R2} - \tau_{R1})}\sum_{n}\frac{2}{n\pi}(-1)^{n+2}\sin(n\pi\psi)A_n \quad (20)$$

where A_n is given by

$$A_n = \left(\tau_{R2} + \frac{1}{\bar{\alpha}n^2\pi^2}\right)\exp(-\bar{\alpha}n^2\tau_{R2}) - \left(\tau_{R1} + \frac{1}{\bar{\alpha}n^2\pi^2}\right)\exp(-\bar{\alpha}n^2\tau_{R1}) \quad (21)$$

In order to obtain a dependable value of α, eq 12 is fitted to the experimental data in that window of ψ and τ where sensitivity, defined by eqs 17 and 20, is high. In addition, uncertainty in the estimated properties is determined by conducting statistically independent experiments.

IV. MATERIALS, SAMPLE PREPARATION, AND EXPERIMENTAL PROTOCOL

In the present study, we use an aqueous suspension of Laponite JS (sodium magnesium fluorosilicate), which is a sol forming variant of Laponite clay.[45] Laponite particles are disklike with 25 nm diameter and 1 nm thickness with very little size/shape distribution.[46] In a single layer of Laponite, two tetrahedral silica layers sandwich an octahedral magnesia layer.[47] A particle of Laponite can, therefore, be considered as a single crystal. The face of a Laponite particle is negatively charged while the edge

dx.doi.org/10.1021/ie402508x | Ind. Eng. Chem. Res. 2013, 52, 15114−15123

Table 1. Ionic Conductivity and pH of Laponite JS Suspension

		concentration of Laponite JS (volume %)				
	initial water + NaOH (10 pH) solution	0.6	1	1.4	2.4	4
pH	10	9.996	9.983	9.917	9.993	10
conductivity (mS/cm)	2.911×10^{-2}	1.933	2.995	3.738	6.205	8.984

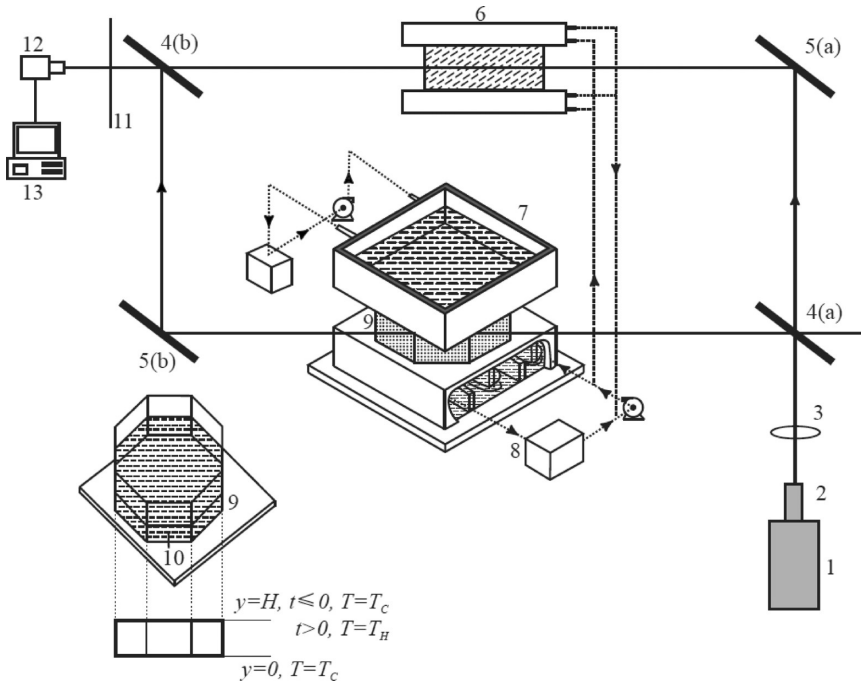

Figure 1. Schematic drawing of a differentially heated test cell integrated with the Mach–Zehnder interferometer: 1, laser; 2, spatial filter; 3, plano convex lens; 4, beam splitters 4(a) and 4(b); 5, mirrors 5(a) and 5(b); 6, compensation chamber; 7, hot water bath; 8, cold water bath; 9, optical cavity; 10, optical window; 11, screen; 12, CCD camera; 13, computer.

has weak positive charge. Laponite JS used in the present work was procured from Southern Clay Products Inc. Laponite JS contains premixed tetrasodium pyrophosphate which prevents aggregation of the particles, thereby providing stability to the sol. It should be noted that, in our previous communication,[29] we had investigated the gel forming grade Laponite RD, which does not have tetrasodium pyrophosphate and therefore transforms into a soft solid with infinite viscosity and finite modulus. The suspension of Laponite JS used in this work, on the other hand, is a free-flowing liquid with viscosity comparable to that of water. According to the manufacturer, suspension of Laponite JS is stable against aggregation over a duration of months for much larger concentrations than used in the present work.[45] A predetermined quantity of white powder of Laponite was mixed with ultrapure water using an ultra Turrex drive as stirrer. Water was maintained at pH 10 to ensure the chemical stability of the Laponite particles.[48] Laponite JS forms a stable and clear suspension in water that remains unaltered for several months. Laponite JS suspension prepared using this procedure was used for rheology and interferometry experiments. The ionic conductivity and pH of the suspension after incorporation of Laponite JS are reported in Table 1. While the pH remains practically constant, the conductivity increases as expected with Laponite concentration.

Rheological experiments were carried out in a concentric cylinder geometry (diameter of inner cylinder, 26.663 mm, and thickness of the annular region, 1.08 mm) using an Anton Paar MCR 501 rheometer (stress controlled rheometer with minimum torque of 0.02 ± 0.001 μNm). Viscosity is measured over a range of shear rates from 25/s to 140/s and is observed to be constant over this range. We ensured the absence of Taylor–Couette instability in the annular gap during the measurement of viscosity over this shear rate range.

Transient heat transfer experiments were performed using a Mach–Zehnder interferometer. A schematic drawing of the setup is shown in Figure 1. In this setup the collimated laser beam [632.8 nm, 35 mW He–Ne laser (Spectra Physics)] is split using a beam splitter and passed through the test and reference chambers as shown in Figure 1. Subsequently, the beams are superimposed, and the resulting image is recorded by a CCD camera. Owing to the optical path difference generated between the beams passing through the test and reference sections, an interference pattern is formed. Before beginning the experiment, the test chamber was filled with Laponite JS suspension having a certain concentration. The reference chamber was filled with glucose solution. The concentration of the glucose solution in the reference chamber was varied in such a way that it matched the refractive index of Laponite suspension in the test chamber at temperature T_C. This step ensured balancing of the optical path lengths of the light beams passing through the reference and test chambers. Superposition of the two light beams resulted in constructive interference with a bright spot on the screen. This state of the interferometer is referred to as the infinite fringe setting. Subsequent to attainment of thermal equilibrium between the test and reference sections of the apparatus, the temperature of the

dx.doi.org/10.1021/ie402508x | Ind. Eng. Chem. Res. 2013, 52, 15114–15123

top plate was raised to T_H. Soon after the top plate temperature was raised to T_H, heat diffused toward the lower surface, causing an increase in temperature within the medium. Consequently, the refractive index of the suspension was altered, generating an optical path difference between the beams passing through the test and reference chambers. Superposition of the two light beams leads to an interference pattern.

In the present set of experiments, we maintained T_C between 19 and 20 °C, while T_H is varied between 21 and 23 °C. The horizontal bounding surfaces of the test cell were made of 1.6 mm copper sheets. Temperatures were maintained constant by circulating water over these surfaces from constant temperature baths. The lower surface was baffled to form a tortuous flow path in addition to creating a fin effect. Constant temperature baths maintained temperature constant to within ±0.1 °C. Direct measurement by thermocouples did not reveal any (measurable) spatial temperature variation. These temperatures were constant to within ±0.1 °C during the experimental duration of 4−5 h. Experiments were carried out in an air-conditioned room where temperature was constant to within ±1.0 °C. The bounding surfaces reached their respective temperatures in 1−2 min. This delay is negligible in comparison to the experimental duration of 4−5 h. The time constant of the diffusion process can be estimated as $H^2/\alpha \sim$ 4.6 h.

We study below the effect of concentration of Laponite JS up to 4 vol % in water. For each concentration, a minimum of three experiments was carried out to examine repeatability. In order to analyze results of the laser interferometry, the temperature dependence of the refractive index of the Laponite suspension at each concentration is required. In the present work, a refractometer (Abbemat 500, Anton Paar) was used to measure the refractive index of the suspension at various temperatures.

V. RESULTS AND DISCUSSION

Viscosity of the Suspension. In Figure 2 we plot the effective viscosity of the aqueous suspension as a function of the volume fraction of Laponite JS. It can be seen that the viscosity, shown as circles, increases with the volume fraction, such that, for 4% volume fraction of Laponite, the viscosity is 3 times that of water. Note that the uncertainty band is quite small. In section II we discussed the need to enforce a limit of $Pe \ll 1$ to ensure random (isotropic) orientation of the clay disks for eq 1 to hold. This assumption can now be examined. For $\eta_s = 10^{-3}$ Pa·s, $d = 25$ nm, $\dot{\gamma} = 100$/s, and $T = 300$ K, we get $Pe \approx 0.0005$, which is considerably smaller than unity. Hence, the particle orientation is randomized and there are no preferred directions for thermal diffusivity. Further, the system is gravitationally stable (bottom heavy) and convection is not present. Hence, random orientation of the original medium is preserved during the conduction heat transfer experiment.

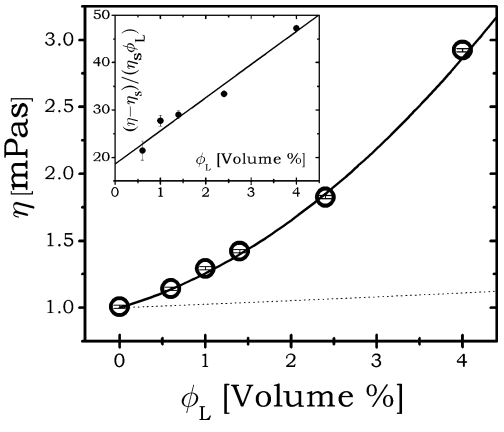

Figure 2. Viscosity (open circles) of suspension is plotted as a function of volume % of Laponite JS in water obtained at 25 °C. The solid line is a fit of eq 1 for oblate particle suspension. The dotted line is the prediction of the viscosity of the suspension having spherical particles. In the inset, $(\eta - \eta_s)/(\eta_s\phi_L)$ is plotted as a function of volume % Laponite. The solid line in the inset is the same fit of eq 1 shown in the main figure. The intercept of the line on the vertical axis (limit of $\phi_L \rightarrow 0$) is the intrinsic viscosity.

It can be seen that eq 1 fits the data very well, which is represented by a solid line in Figure 2. In the inset of Figure 2 we plot $(\eta - \eta_s)/(\eta_s\phi_L)$ as a function of concentration of Laponite. The linear fit to the data in the inset by rearranged eq 1 is given by $(\eta - \eta)/(\eta_s\phi_L) = [\eta]_0 + C_2\phi$, whose intercept on the vertical axis leads to the intrinsic viscosity $[\eta]_0$. Equation 2 relates the intrinsic viscosity $[\eta]_0$ to the aspect ratio of oblate particles. Remarkably the value of $[\eta]_0 = 18.62$ obtained from the linear fit leads to $1/r_p = 25.7$, which is very close to the value of 25 reported in the literature from independent measurements.[45,46] The fit of the data also yields the Huggins coefficient $k_H = 2$ for disklike particles of Laponite. Importantly, a good fit of the experimental data is obtained to the viscosity relation based on classical theory. It confirms the aspect ratio of the particle independently and rules out the presence of clusters of disklike particles within the suspension. For this reason, measured thermal conductivity data in the section Thermal Conductivity of the Suspension have been compared with the well-established models of Hamilton and Crosser and Fricke.

Thermal Diffusivity of the Suspension. Next, we discuss thermal diffusivity measurements based on interferometry experiments. Subsequent to a step increase in temperature of the top surface, one-dimensional diffusion of heat is initiated toward the cold plate of the test section. An increase in temperature of the suspension changes its density and, hence, the refractive index. This alters the optical path length of the beam of light passing through the test section in comparison with the reference, producing an interference pattern on superposition. It is noted here that diffusivity changes in the range 21−23 °C are small enough from a modeling perspective (eq 12). However, density and refractive index changes are large enough to create a measurable optical path difference needed for the formation of interferograms. Measurement sensitivity is further enhanced by having a test cell that is long in the viewing direction.

The time evolution of the interference pattern is shown in Figure 3. In the beginning, the fringe pattern at time $t = 0$ reveals an infinite fringe setting, corresponding to constructive interference when equal path lengths are obtained in the light beam passing through the test and reference sections. As heat diffuses from the top surface into the suspension, fringes appear in its neighborhood and migrate with time toward the lower surface. In the limit of large times, steady state sets in and fringes get distributed throughout the field. The temperature difference associated with two consecutive fringes (ΔT_ε) can be estimated from the knowledge of variation of the refractive index with temperature dn/dT, wavelength of light λ, and length of the test cell L, and is given by principles of wave optics as[49]

dx.doi.org/10.1021/ie402508x | Ind. Eng. Chem. Res. 2013, 52, 15114−15123

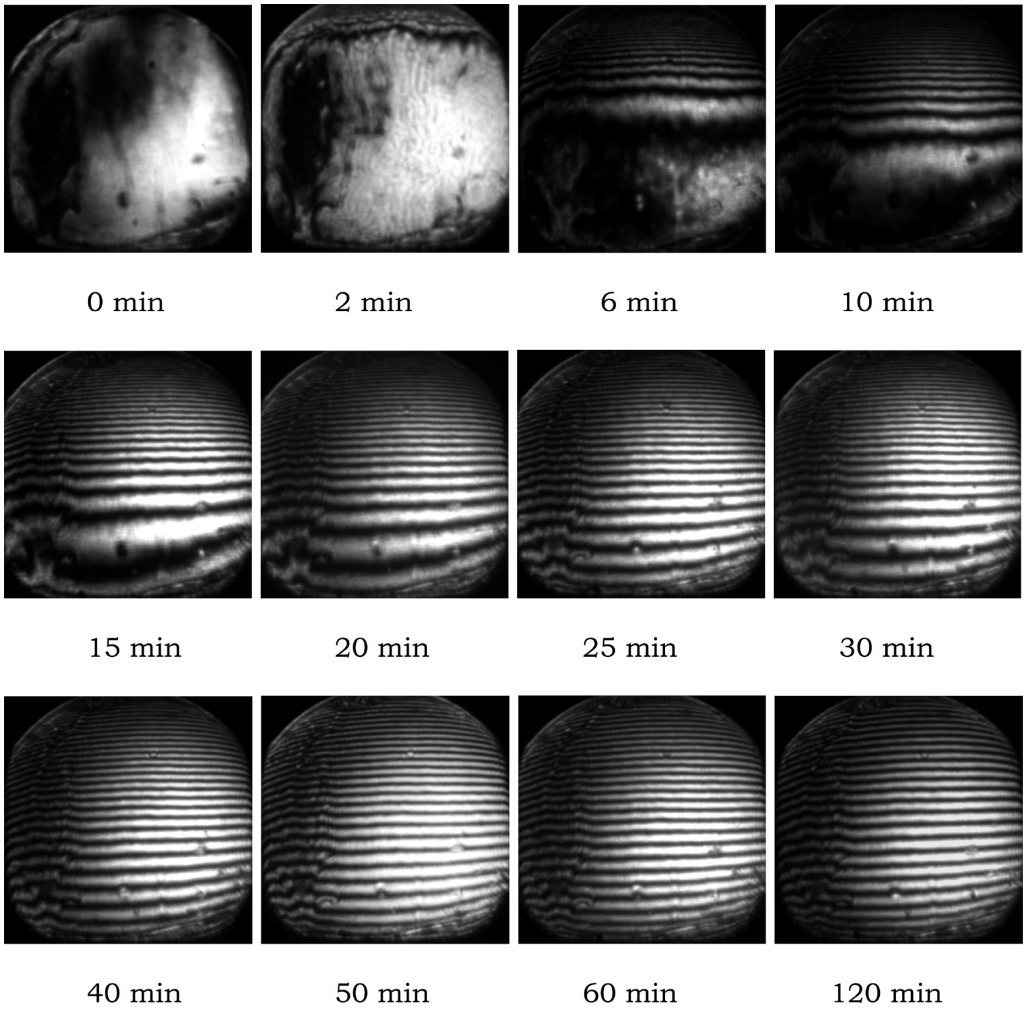

Figure 3. Evolution of interference pattern as a function of time for 2.4 vol % aqueous Laponite JS suspension. The upper and lower surfaces were maintained at 21.7 and 19.7 °C, respectively.

$$\Delta T_{\varepsilon} = \lambda/(L\ \mathrm{d}n/\mathrm{d}T) \tag{22}$$

Equation 22 assumes that the passage of the light ray is straight and beam bending due to refraction is small. Refraction would be strong in the initial stages when the temperature (and, hence, refractive index) gradient near the top wall is large. Explicit calculations with a generalized form[49] of eq 22 showed that, for times greater than 20 min, the refraction error is less than 1% and eq 22 is applicable. This requirement is fulfilled during data analysis in a statistical framework using the sensitivity function. In Figure 4, we plot the evolution of temperature as a function of distance from the top surface and time elapsed in minutes, since the creation of a temperature jump. Prior to the introduction of the jump in temperature, the temperature field is uniform, and equal to the temperature of the lower surface. As heat diffuses through the suspension, a sharp gradient in temperature develops near the top plate. The gradient weakens progressively, and in the limit of long time the steady state sets in.

The evolution of temperature shown in Figure 4 is equivalent to the analytical solution of the diffusion equation given by eq 12. A fit of the analytical solution to the experimental data leads to the determination of the thermal diffusivity, α. However, as discussed in section II, the fit of experimental data in the limit of very short times and very long times is not sensitive to the

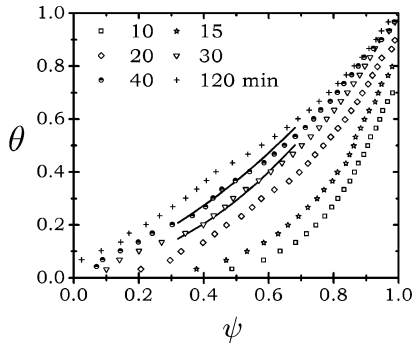

Figure 4. Evolution of normalized temperature (θ) plotted as a function of normalized distance from the bottom plate (ψ) for the interference patterns shown in Figure 3 (2.4 vol %). Symbols represent the experimental data obtained at different times (in minutes), while the lines are fits of the analytical solution (eq 12) at different times to the experimental data. In 90% sensitivity window in time and spatial domain the coefficient of determination (R^2) for the fits for 30 and 40 min data are 0.9826 and 0.9645, respectively.

parametric changes in α and can result in curve-fitting errors. In addition, temperature data close to the isothermal boundaries of the apparatus are also not sensitive to α. Therefore, in order to obtain the appropriate range of times (t or τ) and distance

dx.doi.org/10.1021/ie402508x | Ind. Eng. Chem. Res. 2013, 52, 15114−15123

from the lower surface (y or ψ) to be considered for parameter estimation, we plot $\bar{S}_t$ as a function of τ and $\bar{S}_y$ as a function of ψ in parts a and b, respectively, of Figure 5. It can be seen that

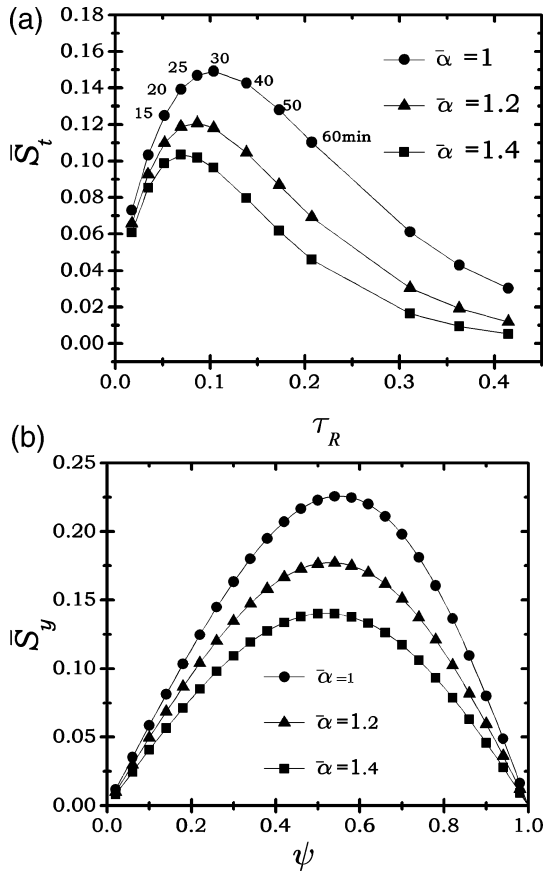

Figure 5. Normalized sensitivities $\bar{S}_t$ and $\bar{S}_y$ plotted as a function of (a) dimensionless time and (b) dimensionless distance from the bottom plate, respectively. In Figure 4 we fit only that part of the data which lies within the 90% of the window of the maximum value.

both sensitivities have a clear maximum, indicating that experimental data should be selectively used for parameter estimation. In Figure 4, we fit eq 12 to only that part of the experimental data which is within the 90% window of the maximum value of each of the sensitivities. This statistical procedure reliably estimates thermal diffusivity as a function of volume fraction of Laponite JS.

Thermal Conductivity of the Suspension. Thermal conductivity enhancement in nanofluids has been a subject of many studies over the past decade. Apart from solvent selection, types of nanoparticles, their sizes, and, to a lesser extent, their shapes have been explored. The measurement technique—point, line or volumetric—influences the conductivity prediction. It is, therefore, not surprising that contradictory opinions have been expressed in the literature. In this context, knowledge of the physicochemical behavior of colloidal suspensions is also necessary. A rigorous study that employs thermal conductivity measurement in a stable suspension of anisotropic particles and comparison with available theories helps in further understanding of the subject.

We obtain the thermal conductivity of the suspension using fitted values of thermal diffusivity. The two are related as $k = \rho C_P \alpha$, where ρ is the density of the suspension while C_P is its heat capacity at constant pressure. The heat capacity of Laponite clay is known to be 1.03 kJ/(kg·K),[38,39] while that of water is 4.18 kJ/(kg·K). The heat capacity of the suspension is estimated by using the rule of mixtures:[50,51]

$$C_{P,\mathrm{sus}} = w_{\mathrm{L}} C_{P,\mathrm{L}} + w_{\mathrm{W}} C_{P,\mathrm{W}} \tag{23}$$

where w is the mass fraction, C_P is the heat capacity at constant pressure, and subscripts "L" and "W" represent Laponite and water, respectively. In Figure 6 we plot the thermal conductivity

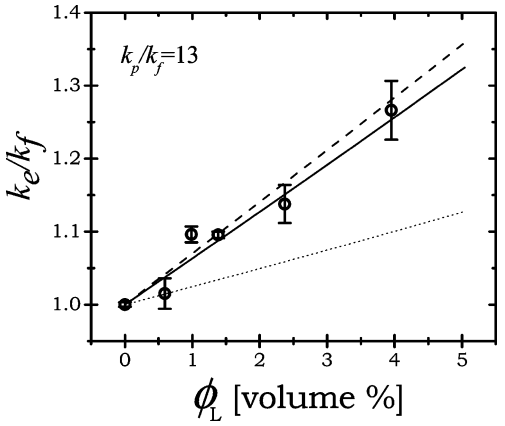

Figure 6. Thermal conductivity as a function of concentration of Laponite JS. Symbols represent the experimental data, the solid line represents the analytical solution due to Fricke (eqs 4–7), and the dashed line represents the analytical expression due to Hamilton and Crosser (eqs 4, 8, and 9) for r_p = 1/25. The dotted line is a solution of the Maxwell equation (eq 4) for suspension of spherical particles (n = 3). For all the cases conductivity ratio is k_p/k_f = 13.

of the suspension normalized by the thermal conductivity of water as a function of the volume fraction of Laponite. It can be seen that the thermal conductivity increases with an increase in the concentration of Laponite. An increase of around 30% is observed for a volume fraction of 4%.

In section II, we describe models for the thermal conductivity proposed by Fricke[2] and Hamilton and Crosser[3] for a Brownian suspension of disklike particles. Accordingly, the effective thermal conductivity of the suspension is represented by eqs 4–7 and eqs 4, 8, and 9, respectively. In order to estimate the effective thermal conductivity, the thermal conductivity of a single particle of Laponite is necessary, which is not available in the literature. In addition, owing to its nanoscopic size and anisotropic shape, it is expected that the thermal conductivity of the Laponite crystal would be difficult to measure using conventional techniques. Owing to a layered structure of the particle, comprising outer silica layers that sandwich a magnesia layer, a particle of Laponite is expected to have a high thermal conductivity.

In Figure 6, we plot fits of the Fricke model (eqs 4–7) and the Hamilton and Crosser model (eqs 4, 8, and 9) to the experimental data. It can be seen that each model shows a good fit to the suspension thermal conductivity for k_p/k_f = 13. Since the thermal conductivity of water is 0.58 W/(m·K), the estimated thermal conductivity of the Laponite particle comes out to be around 7.54 W/(m·K). Interestingly, crystalline silica is known to have a thermal conductivity of 14 W/(m·K).[52] This suggests that the estimated value of the thermal conductivity of Laponite particle is plausible. Figure 6 also shows the prediction of the Maxwell model (eq 4) for suspension of isotropic particles (n = 3) for k_p/k_f = 13. It can be seen that, owing to

dx.doi.org/10.1021/ie402508x | Ind. Eng. Chem. Res. 2013, 52, 15114–15123

anisotropy, the Laponite JS suspension shows substantial improvement over the suspension of isotropic particles that obey Maxwellian behavior. As discussed previously, such an enhancement can be attributed to increased thermal transport due to greater length scale and surface area associated with anisotropic particles than that of isotropic particles.

As discussed in section I, a significant amount of research in the literature reports the effect of incorporation of nanoparticles in liquid media on the thermal conductivity. Some studies claim an anomalous increase in the thermal conductivity that cannot be explained by the existing effective medium theories. It is now believed that an anomalous enhancement can be attributed to the formation of a cluster with fractal-like behavior. In the present work, an excellent fit of the viscosity relation based on two-body interaction to the experimental data rules out the possibility of cluster formation.

The thermal conductivity data based on unsteady heat conduction is less conclusive. The degree of enhancement of the thermal conductivity of the aqueous suspension of Laponite and its match with theory relies on the knowledge of the particle thermal conductivity. The possibility of an anomalous increase can be ruled out only with an independent estimation of the thermal conductivity of the Laponite particle. Nonetheless, qualitative agreement of the Fricke model and the Hamilton and Crosser model with experimental data is encouraging. In view of the fact that the estimated value of the Laponite thermal conductivity is plausible, reference to any other mechanism to support anomalous enhancement is not necessary. Following the correct prediction of viscosity, the effective medium theory may now be taken as applicable in the context of energy transfer. Consequently, the theoretical models combined with the measured thermal diffusivity data provide a method of estimating the particle thermal conductivity itself.

Thermal Fluctuations. The role of Brownian motion in the enhancement of the thermal conductivity has been assessed thoroughly in the literature. Careful analysis by Fan and Wang[9] (and references therein) clearly rule out this possibility. On thermophoresis, Piazza and Parola[53] discuss the thermophoretic diffusivity to be comparable to (or smaller than) the mass diffusivity of Laponite in water. The mass diffusivity itself is several orders of magnitude smaller than the thermal diffusivity. In addition, the gradient of temperature in the thermal cell used in the present work is small, being around 2 K at 300 K over a distance of 50 mm. These factors suggest that thermophoresisis has a negligible contribution to the overall heat transport.

Anisotropic particles at the nanoscale have significant advantages over microscopic particles. Owing to their small size, thermal fluctuations of internal energy eliminate chances of sedimentation and enhance the stability of the suspension. Furthermore, thermal factors keep small anisotropic particles isotropically oriented, making thermal conductivity an isotropic quantity. Larger anisotropic particles, on the other hand, would take longer to randomize their orientation.

VI. CONCLUSIONS

We measure the viscosity of an aqueous suspension of Laponite JS and observe that it increases with particle concentration. Effective medium theory for viscosities of suspensions of anisotropic particles fits the experimental data very well. In addition, the intrinsic viscosity estimated from the fit correctly predicts the aspect ratio of the Laponite particles. This suggests the absence of formation of any particle clusters in the suspension. We measure the thermal diffusivity from a transient heat conduction experiment using laser light interferometry, wherein the temperature dependence of the refractive index of the suspension is utilized for image formation. Typically, for incorporation of 4 vol % of nanodisks, around 30% enhancement in the thermal conductivity is observed in the temperature range 21−23 °C. Similar enhancements can be expected at other temperatures that are close to the ambient. The Fricke model as well as the Hamilton and Crosser model for the thermal conductivity of suspension of anisotropic particles explains the trend of the experimental data quite well. The fit requires information of the particle thermal conductivity. A retrieved value of the Laponite thermal conductivity is seen to be realistic.

AUTHOR INFORMATION

Corresponding Author

*E-mail: joshi@iitk.ac.in.

Notes

The authors declare no competing financial interest.

ACKNOWLEDGMENTS

This work was supported by Department of Science and Technology, Government of India.

REFERENCES

(1) Deen, W. M. *Analysis of Transport Phenomena*; Oxford University Press: New York, 1998.

(2) Fricke, H. A Mathematical Treatment of the Electric Conductivity and Capacity of Disperse Systems I. The Electric Conductivity of a Suspension of Homogeneous Spheroids. *Phys. Rev.* **1924**, *24*, 575.

(3) Hamilton, R. L.; Crosser, O. K. Thermal Conductivity of Heterogeneous Two-Component Systems. *Ind. Eng. Chem. Fundam.* **1962**, *1*, 187.

(4) Chopkar, M.; Sudarshan, S.; Das, P.; Manna, I. Effect of Particle Size on Thermal Conductivity of Nanofluid. *Metall. Mater. Trans. A* **2008**, *39A*, 1535.

(5) Pilkington, G. A.; Briscoe, W. H. Nanofluids Mediating Surface Forces. *Adv. Colloid Interface Sci.* **2012**, *179−182*, 68.

(6) Gao, J. W.; Zheng, R. T.; Ohtani, H.; Zhu, D. S.; Chen, G. Experimental Investigation of Heat Conduction Mechanisms in Nanofluids. Clue on Clustering. *Nano Lett.* **2009**, *9*, 4128.

(7) Maxwell, J. C. *A Treatise on Electricity and Magnetism*; Clarendon Press: Oxford, 1891.

(8) Eastman, J. A.; Phillpot, S. R.; Choi, S. U. S.; Keblinski, P. Thermal Transport in Nanofluids. *Annu. Rev. Mater. Res.* **2004**, *34*, 219.

(9) Fan, J.; Wang, L. Review of Heat Conduction in Nanofluids. *J. Heat Transfer* **2011**, *133*, 040801.

(10) Keblinski, P.; Prasher, R.; Eapen, J. Thermal Conductance of Nanofluids: Is the Controversy Over? *J. Nanopart. Res.* **2008**, *10*, 1089.

(11) Kleinstreuer, C.; Feng, Y. Experimental and Theoretical Studies of Nanofluid Thermal Conductivity Enhancement: A Review. *Nanoscale Res. Lett.* **2011**, *6*, 229.

(12) Kumar, D. H.; Patel, H. E.; Kumar, V. R. R.; Sundararajan, T.; Pradeep, T.; Das, S. K. Model for Heat Conduction in Nanofluids. *Phys. Rev. Lett.* **2004**, *93*, 144301.

(13) Choi, S. U. S.; Zhang, Z. G.; Yu, W.; Lockwood, F. E.; Grulke, E. A. Anomalous Thermal Conductivity Enhancement in Nanotube Suspensions. *Appl. Phys. Lett.* **2001**, *79*, 2252.

(14) Prasher, R.; Phelan, P. E.; Bhattacharya, P. Effect of Aggregation Kinetics on the Thermal Conductivity of Nanoscale Colloidal Solutions (Nanofluid). *Nano Lett.* **2006**, *6*, 1529.

(15) Shalkevich, N.; Escher, W.; Buergi, T.; Michel, B.; Ahmed, L.; Poulikakos, D. On the Thermal Conductivity of Gold Nanoparticle Colloid. *Langmuir* **2010**, *26*, 663.
(16) Buongiorno, J.; Venerus, D. C.; Prabhat, N.; McKrell, T.; Townsend, J.; Christianson, R.; Tolmachev, Y. V.; Keblinski, P.; Hu, L. W.; Alvarado, J. L.; Bang, I. C.; Bishnoi, S. W.; Bonetti, M.; Botz, F.; Cecere, A.; Chang, Y.; Chen, G.; Chen, H.; Chung, S. J.; Chyu, M. K.; Das, S. K.; Di Paola, R.; Ding, Y.; Dubois, F.; Dzido, G.; Eapen, J.; Escher, W.; Funfschilling, D.; Galand, Q.; Gao, J.; Gharagozloo, P. E.; Goodson, K. E.; Gutierrez, J. G.; Hong, H.; Horton, M.; Hwang, K. S.; Iorio, C. S.; Jang, S. P.; Jarzebski, A. B.; Jiang, Y.; Jin, L.; Kabelac, S.; Kamath, A.; Kedzierski, M. A.; Kieng, L. G.; Kim, C.; Kim, J. H.; Kim, S.; Lee, S. H.; Leong, K. C.; Manna, I.; Michel, B.; Ni, R.; Patel, H. E.; Philip, J.; Poulikakos, D.; Reynaud, C.; Savino, R.; Singh, P. K.; Song, P.; Sundararajan, T.; Timofeeva, E.; Tritcak, T.; Turanov, A. N.; Van Vaerenbergh, S.; Wen, D.; Witharana, S.; Yang, C.; Yeh, W. H.; Zhao, X. Z.; Zhou, S. Q. A Benchmark Study on the Thermal Conductivity of Nanofluids. *J. Appl. Phys.* **2009**, *106*, 094312.
(17) Keblinski, P.; Phillpot, S. R.; Choi, S. U. S.; Eastman, J. A. Mechanisms of Heat Flow in Suspensions of Nano-sized Particles (Nanofluids). *Int. J. Heat Mass Transfer* **2002**, *45*, 855.
(18) Assael, M. J.; Chen, C. F.; Metaxa, I.; Wakeham, W. A. Thermal Conductivity of Suspensions of Carbon Nanotubes in Water. *Int. J. Thermophys.* **2004**, *25*, 971.
(19) Assael, M. J.; Metaxa, I. N.; Arvanitidis, J.; Christofilos, D.; Lioutas, C. Thermal Conductivity Enhancement in Aqueous Suspensions of Carbon Multi-walled and Double-walled Nanotubes in the Presence of Two Different Dispersants. *Int. J. Thermophys.* **2005**, *26*, 647.
(20) Ding, Y.; Alias, H.; Wen, D.; Williams, R. Heat Transfer of Aqueous Suspensions of Carbon Nanotubes (CNT Nanofluids). *Int. J. Heat Mass Transfer* **2006**, *49*, 240.
(21) Liu, M.-S.; Lin, M. C.-C.; Huang, I-T.; Wang, C.-C. Enhancement of Thermal Conductivity with Carbon Nanotube for Nanofluids. *Int. Commun. Heat Mass Transfer* **2005**, *32*, 1202.
(22) Xie, H.; Lee, H.; Youn, W.; Choi, M. Nanofluids Containing Multiwalled Carbon Nanotubes and Their Enhanced Thermal Conductivities. *J. Appl. Phys.* **2003**, *94*, 4967.
(23) Biercuk, M. J.; Llaguno, M. C.; Radosavljevic, M.; Hyun, J. K.; Johnson, A. T.; Fischer, J. E. Carbon Nanotube Composites for Thermal Management. *Appl. Phys. Lett.* **2002**, *80*, 2767−2769.
(24) Putnam, S. A.; Cahill, D. G.; Braun, P. V.; Ge, Z.; Shimmin, R. G. Thermal Conductivity of Nanoparticle Suspensions. *J. Appl. Phys.* **2006**, *99*, 084308.
(25) Cherkasova, A. S.; Shan, J. W. Particle Aspect-Ratio Effects on the Thermal Conductivity of Micro- and Nanoparticle Suspensions. *J. Heat Transfer* **2008**, *130*, 082406.
(26) Nan, C. W.; Birringer, R.; Clarke, D. R.; Gleiter, H. Effective Thermal Conductivity of Particulate Composites with Interfacial Thermal Resistance. *J. Appl. Phys.* **1997**, *81*, 6692.
(27) Singh, D.; Timofeeva, E.; Yu, W.; Routbort, J.; France, D.; Smith, D.; Lopez-Cepero, J. An Investigation of Silicon Carbide-Water Nanofluid for Heat Transfer Applications. *J. Appl. Phys.* **2009**, *15*, 064306.
(28) Khandekar, S.; Joshi, Y. M.; Mehta, B. Thermal Performance of Closed Two-Phase Thermosyphon Using Nanofluids. *Int. J. Therm. Sci.* **2008**, *47*, 659.
(29) Bhandari, S. S.; Muralidhar, K.; Joshi, Y. M. Enhanced Thermal Transport Through a Soft Glassy Nanodisk Paste. *Phys. Rev. E* **2013**, *87*, 022301.
(30) Kole, M.; Dey, T. K. Investigation of Thermal Conductivity, Viscosity, and Electrical Conductivity of Graphene Based Nanofluids. *J. Appl. Phys.* **2013**, *113*, 084307.
(31) Baby, T. T.; Ramaprabhu, S. Enhanced Convective Heat Transfer Using Graphene Dispersed Nanofluids. *Nanoscale Res. Lett.* **2011**, *6*, 289.
(32) Ghozatloo, A.; Shariaty-Niasar, M.; Rashidi, A. M. Preparation of Nanofluids from Functionalized Graphene by New Alkaline Method and Study on the Thermal Conductivity and Stability. *Int. Commun. Heat Mass Transfer* **2013**, *42*, 89.
(33) Yu, W.; Xie, H.; Wang, X. Significant Thermal Conductivity Enhancement for Nanofluids Containing Graphene Nanosheets. *Phys. Lett. A* **2011**, *375*, 1323.
(34) Sun, Z.; Pöller, S.; Huang, X.; Guschin, D.; Taetz, C.; Ebbinghaus, P.; Masa, J.; Erbe, A.; Kilzer, A.; Schuhmann, W.; Muhler, M. High-yield Exfoliation of Graphite in Acrylate Polymers: A Stable Few-layer Graphene Nanofluid with Enhanced Thermal Conductivity. *Carbon* **2013**, *64*, 288.
(35) Wang, F.; Han, L.; Zhang, Z.; Fang, X.; Shi, J.; Ma, W. Surfactant-free Ionic Liquid-Based Nanofluids with Remarkable Thermal Conductivity Enhancement at Very Low Loading of Graphene. *Nanoscale Res. Lett.* **2012**, *7*, 314.
(36) Dhar, P.; Sen Gupta, S.; Chakraborty, S.; Pattamatta, A.; Das, S. K. The Role of Percolation and Sheet Dynamics During Heat Conduction in Poly-dispersed Graphene Nanofluids. *Appl. Phys. Lett.* **2013**, *102*, 163114.
(37) Martin-Gallego, M.; Verdejo, R.; Khayet, M.; de Zarate, J. M. O.; Essalhi, M.; Lopez-Manchado, M. A. Thermal Conductivity of Carbon Nanotubes and Graphene in Epoxy Nanofluids and Nanocomposites. *Nanoscale Res. Lett.* **2011**, *6*, 1.
(38) Larson, R. G. *The Structure and Rheology of Complex Fluids*; Clarendon Press: Oxford, 1999.
(39) Batchelor, G. K.; Green, J. T. The Determination of the Bulk Stress in a Suspension of Spherical Particles to Order c2. *J. Fluid Mech.* **1972**, *56*, 401.
(40) Batchelor, G. K. The Effect of Brownian Motion on the Bulk Stress in a Suspension of Spherical Particles. *J. Fluid Mech.* **1977**, *83*, 97.
(41) van der Kooij, F. M.; Boek, E. S.; Philipse, A. P. Rheology of Dilute Suspensions of Hard Platelike Colloids. *J. Colloid Interface Sci.* **2001**, *235*, 344.
(42) Low, P. F. *Clay-Water Interface and its Rheological Implications*; The Clay Minerals Society: Boulder, CO, 1992.
(43) Chapra, S. C.; Canale, R. P. *Numerical Methods for Engineers*; 5th ed.; McGraw-Hill: New York, 2006.
(44) Ozisik, M. N.; Orlande, H. R. B. *Inverse Heat Transfer: Fundamentals and Applications*; Taylor and Francis: New York, 2000.
(45) http://www.laponite.com.
(46) Kroon, M.; Wegdam, G. H.; Sprik, R. Dynamic Light Scattering Studies on the Sol-Gel Transition of a Suspension of Anisotropic Colloidal Particles. *Phys. Rev. E* **1996**, *54*, 6541.
(47) Shahin, A.; Joshi, Y. M. Physicochemical Effects in Aging Aqueous Laponite Suspensions. *Langmuir* **2012**, *28*, 15674.
(48) Thompson, D. W.; Butterworth, J. T. The Nature of Laponite and its Aqueous Dispersions. *J. Colloid Interface Sci.* **1992**, *151*, 236.
(49) Goldstein, R. J. *Fluid Mechanics Measurements*; 2nd ed.; Taylor and Francis: New York, 1996.
(50) Buongiorno, J. Convective Transport in Nanofluids. *J. Heat Transfer* **2005**, *128*, 240.
(51) O'Hanley, H.; Buongiorno, J.; McKrell, T.; Hu, L.-w. Measurement and Model Validation of Nanofluid Specific Heat Capacity with Differential Scanning Calorimetry. *Adv. Mech. Eng.* **2012**, *2012*, 181079.
(52) Ardebili, H.; Pech, M. *Encapsulation Technologies for Electronic Applications*; Elsevier: Oxford, 2009.
(53) Piazza, R.; Parola, A. Thermophoresis in Colloidal Suspensions. *J. Phys.: Condens. Matter* **2008**, *20*, 153102.